Constraining the date of a seasonally ice-free Arctic using a simple model

David B. Bonan[1], Tapio Schneider[1], Ian Eisenman[2], Robert C.J. Wills[3]

[1]Environmental Science and Engineering, California Institute of Technology, Pasadena, California, USA
[2]Scripps Institute of Oceanography, University of California San Diego, La Jolla, California, USA
[3]Department of Atmospheric Sciences, University of Washington, Seattle, Washington, USA

Key Points:

- A model relating future SIA to present SIA and local sea-ice sensitivity is used to explain the intermodel spread in Arctic SIA projections

- Biases in simulating present-day SIA contribute most to the intermodel spread with model differences in Arctic warming contributing the rest

- Under high emissions, constraints suggest the Arctic will likely be ice-free in September around 2046 and from July to October around 2059

Corresponding author: David B. Bonan, dbonan@caltech.edu

Abstract

State-of-the-art climate models simulate a large spread in the projected decline of Arctic sea-ice area (SIA) over the 21st century. Here we diagnose causes of this intermodel spread using a model that approximates future SIA based on present SIA and the sensitivity of SIA to Arctic temperatures. This model accounts for 70–95% of the intermodel variance, with the majority of the spread arising from present-day biases. The remaining spread arises from model differences in Arctic warming, with some contribution from the local sea-ice sensitivity. Using observations to constrain the projections moves the probability of an ice-free Arctic forward by 10–35 years. Under a high-emissions scenario, an ice-free Arctic will likely (>66% probability) occur in September around 2046 and from July–October around 2059. Under a medium-emissions scenario, this date occurs around 2051 in September and 2080 from July–October. These observation-based constraints imply ice-free Arctic summers are approaching faster than previously thought.

Plain Language Summary

Arctic sea ice coverage has declined substantially over the past few decades and is projected to continue to decline over the next century. These projections, however, are marred by large uncertainties which arise primarily due to differences between climate models. In this study, we use a simple model that emulates the future evolution of Arctic sea ice as simulated by climate models to explain where this uncertainty comes from. We show that biases in simulating present-day Arctic sea ice contributes most of the uncertainty, with model differences in the simulated amount of Arctic warming contributing much of the rest. We then use observations to constrain our simple model and show that under a high emissions scenario it is likely the Arctic will be free of sea ice in September around 2046 and from July to October around 2059. We also show that the emissions pathway impacts the length of ice free summers in the Arctic. Nonetheless, these results imply ice free summers in the Arctic are approaching faster than previously thought.

1 Introduction

The rapid loss of Arctic sea ice over the last several decades has been one of the clearest manifestations of climate change. Since the beginning of the satellite record, Arctic sea ice has thinned substantially across all seasons, and its summertime coverage has declined by approximately 50% (Fetterer et al., 2016; Stroeve & Notz, 2018). Because sea ice plays an important role in shaping local ecosystems (Wyllie-Echeverria & Wooster, 1998; Laidre et al., 2008), the life of indigenous populations (Ford & Smit, 2004), and socioeconomic activities in the Arctic (Melia et al., 2016), there has been a concerted effort to determine when the Arctic will become seasonally ice free.

Estimates suggest that in September the Arctic will most likely be ice free (< 1 million km^2) by the end of the 21st century (Boé et al., 2009; Notz, 2015; Jahn, 2018; Niederdrenk & Notz, 2018; Sigmond et al., 2018). But it could be ice free as early as mid-century (Holland et al., 2006; Liu et al., 2013; Notz, 2015; Jahn, 2018; Notz & SIMIP Community, 2020; Diebold & Rudebusch, 2021) or in the 2030s (Wang & Overland, 2009; Overland & Wang, 2013; Snape & Forster, 2014; Diebold & Rudebusch, 2021). The large uncertainties in projections of Arctic sea-ice area (SIA) and the date of an ice-free Arctic arise primarily because of structural differences between state-of-the-art global climate models (GCMs) and how they respond to external forcing (Stroeve et al., 2012; Massonnet et al., 2012; Notz & SIMIP Community, 2020; Bonan et al., 2021). Emergent constraints, which rely on statistical relationships between observable aspects of the current climate system and future climate change across GCMs, have been used to reduce this spread (Boé et al., 2009; Massonnet et al., 2012; Hall et al., 2019; Senftleben et al., 2020). They suggest that the Arctic may experience ice free conditions in September at some point between 2045 and 2060. Yet, the factors underpinning some of the proposed emergent constraints are currently poorly understood (Hall et al., 2019); in particular, there has been no satisfactory accounting of the relative importance of the sea ice response to warming versus biases in simulating present-day sea ice.

One conceptually convenient metric to understand Arctic sea-ice changes is the sea ice sensitivity, defined as a change of SIA per degree of global warming (Winton, 2011) or per change in cumulative carbon-dioxide emissions (Notz & Marotzke, 2012; Notz & Stroeve, 2016). Because Arctic SIA has been found to be approximately linearly related to global-mean surface temperatures in individual GCMs (Gregory et al., 2002; Winton, 2011;

Armour et al., 2011; Mahlstein & Knutti, 2012; Rosenblum & Eisenman, 2017), it implies that long-term variations in simulated global warming should be proportional to long-term variations in simulated sea ice retreat, which is indeed seen in GCMs (Mahlstein & Knutti, 2012; Rosenblum & Eisenman, 2016, 2017; Jahn, 2018). This suggests that Arctic SIA at some point in time $A(t)$ can be approximated by

$$A(t) = \overline{A}_c + \gamma \cdot (T(t) - \overline{T}_c) \tag{1}$$

where $\overline{A}_c$ is the climatological SIA in a specific reference period, γ is the sea ice sensitivity, and $T(t) - \overline{T}_c$ is the amount of warming relative to the climatological temperature $\overline{T}_c$ in the reference period. The sea ice sensitivity γ can be obtained from the observational record via regression analysis (e.g., Niederdrenk & Notz, 2018). GCMs suggest, at least for annual-mean data, that γ is fairly constant in time (Winton, 2011; Mahlstein & Knutti, 2012), implying that the observational record can be used to estimate the true sea ice sensitivity. However, because SIA relates more directly to Arctic warming than to global warming (Olonscheck et al., 2019), we go a step further and interpret $T(t) - \overline{T}_c$ as Arctic (60°N–90°N) temperature changes instead of as global temperature changes. We therefore interpret γ as the *local* sea ice sensitivity, defined as a change of SIA per degree of Arctic warming. Variations in annual Arctic SIA from 1979–2020 are well approximated by this expression given observed Arctic surface temperature variations and an estimated (total least squares regression) local sea ice sensitivity $\gamma = -0.79 \times 10^6$ km^2 °C^{-1} (Fig. 1a). The expression accounts for not only the long-term trend and year-to-year variations ($r = 0.96$), but also the detrended variability ($r = 0.81$), which is thought to be crucial for determining when the Arctic will be ice free (Jahn et al., 2016; Screen & Deser, 2019). From 1979–2020, Eq. (1) with monthly estimates of γ also accounts for variations in SIA at monthly timescales, capturing the large downward trend of Arctic SIA in the summer, the more muted decline in the winter, and the interannual variations of Arctic SIA across all months (Fig. 1c and 1d). However, on monthly timescales, it is less clear if the observed local sea ice sensitivity remains constant in time (Mahlstein & Knutti, 2012).

That Eq. (1) captures the trend and variability of observed Arctic SIA over the past few decades suggests that it could also be used to explain the behavior of coupled GCMs. According to Eq. (1), the spread among GCMs could arise from differences in the mean-state SIA of each GCM ($\overline{A}_c$), in the sensitivity of sea ice to Arctic temperature changes (γ), or in the amount of Arctic warming $T(t) - \overline{T}_c$. What can we make of the intermodel spread in projections of Arctic SIA, and how does each term contribute to the total uncertainty?

If, for instance, mean-state biases were reduced across GCMs, how much more certain is the date of an ice-free Arctic? To address these questions, we use Eq. (1) to introduce a simple framework for partitioning model uncertainty in 21st century projections of Arctic SIA into contributions from these different factors. We then use observations to constrain the individual factors, which facilitates conclusions regarding the probability of seeing an ice-free Arctic in the coming decades.

2 Sources of uncertainty in model projections of Arctic sea ice

We first apply Eq. (1) to simulations in Phase 6 of the Coupled Model Intercomparison Project (CMIP6) (Eyring et al., 2016) with Historical and SSP5-8.5 forcing (details in Methods). Over all months, the proportion of variance across the GCMs that Eq. (1) accounts for varies between 70% and 95% during 2020–2100 (Fig. 2a). The period in which Eq. (1) accounts for the lowest fraction of intermodel variance occurs in early summer during the beginning of the 21st century, when approximately 70–80% of the intermodel variance is captured. Eq. (1) accounts for the most (>90%) intermodel variance in late fall and early winter, likely because model-to-model variations in climatological Arctic SIA are largest in the wintertime (Davy & Outten, 2020; Shu et al., 2020). Arctic SIA calculated from Eq. (1) also bears a striking similarity to the trajectory of each individual GCM for the summer months (Supplemental Figure S1), which is the primary season of interest in this study.

The ability of Eq. (1) to capture most of the intermodel variance suggests the three terms in Eq. (1) can be used to identify sources of intermodel spread in projections of Arctic SIA. Isolating the intermodel spread of each term (details in Methods) shows that in the near future, biases in present-day SIA ($\overline{A}_c$) account for approximately 70–80% of the total intermodel variance (Fig. 2b). In winter, the effect of mean-state biases persists much longer into the 21st century than in the summer, largely because sea ice remains present, whereas summer sea ice disappears in most GCMs by 2065. In summer, mean-state biases are important initially, accounting for 40–50% of the intermodel spread for the first decade beyond 2020, but their contribution quickly diminishes to approximately 20–30% by 2050. The remaining intermodel spread arises from differences in local sea ice sensitivities (Fig. 2c) and Arctic warming (Fig. 2d). In late fall, model differences in the local sea ice sensitivity account for approximately 30% of the intermodel variance at the end of the 21st century. Notably, at the summer minimum, the spread in local sea ice sensitivity explains

little intermodel variance at the end of the 21st century. The majority of the intermodel spread in September Arctic SIA projections at the end of the 21st century is associated with differences in Arctic warming simulated by GCMs, which accounts for over 80% of the intermodel variance. In winter, variations in Arctic warming begin to matter toward the end of the 21st century and make up approximately 30–40% of the total intermodel variance. Similar results are found for a medium emissions scenario (SSP2-4.5) and a low-emissions scenario (SSP1-2.6), though the relative role of intermodel differences in Arctic warming decreases and accounts for 40–60% of the total summer variance by the end of the 21st century (Supplemental Figure S2–S3).

3 Constraining model projections of Arctic sea ice

We can use Eq. (1) in conjunction with observations to constrain the intermodel spread in projections of Arctic SIA. Satellites have been reliably monitoring Arctic sea ice concentration since 1979, giving estimates of Arctic SIA for more than 40 years. Reanalysis datasets similarly give relatively accurate estimates of Arctic temperatures going back to the early 1950s, when the U.S. Navy and other national meteorological institutes began regular, year-round monitoring of the Arctic. We quantify how these observations constrain projections of an ice-free Arctic (defined as the first year when each GCM crosses the 1 million^2 km^2 SIA threshold) by fitting a Gaussian distribution to the GCM ensemble (details in Methods). This is analogous to the cumulative frequencies of GCMs being ice-free.

3.1 September

We begin by focusing on September Arctic SIA projections in GCMs, based on Eq. (1), without observational constraints. Under a high-emissions scenario (SSP5-8.5), CMIP6 GCM estimates for the terms on the right-hand side of Eq. (1) suggest that it is 'likely' (>66% probability) the Arctic will experience an ice-free September by 2057 and that it is 'very likely' (>90% probability) the Arctic will experience an ice-free September around 2100 (Fig. 3a). Raw GCM output predicts that these ice-free dates will occur 3-5 years earlier than Eq. (1) (Supplemental Figure S4), implying that Eq. (1) provides a relatively accurate estimate of the simulated behavior.

Correcting for mean-state biases in GCMs by using Eq. (1) with the mean-state of September Arctic SIA from 1979–2020 in observations rather than GCMs, brings forward

the 'likely' date by 4 years to 2053 and brings forward the 'very likely' by 30 years (Figure 3a). Note, this mean-state adjustment reduces the likelihood of seeing ice-free conditions in the next few decades. Next, using the observed local sea ice sensitivity γ, rather than that from each GCM in addition to the mean-state correction, moves the 'likely' date of an ice-free Arctic forward by three more years to 2050. The 'very likely' date moves forward by an additional 6 years to 2060. This indicates that GCMs tend to underestimate the observed local sea ice sensitivity in September.

The monthly local sea ice sensitivity is not constant in time in the GCM simulations; they systematically show increasingly negative values in the future. The more negative γ values could arise from the fact that the relationship between sea ice thickness and area is not perfectly linear. At higher thickness regimes, a change in Arctic temperature would result in a smaller area change, whereas at lower thickness regimes, the same change in Arctic temperature would result in a larger area change. Estimating γ from 1979 up until a particular year yields an estimate of how the local sea ice sensitivity evolves in the future according to state-of-the-art GCMs (see Methods). With this added guidance, the 'likely' date of seeing an ice-free Arctic in September moves forward by 4 years to 2046. This constraint moves forward the 'very likely' date of ice free conditions in September by 5 years to 2055, which is close to 50 years sooner than the CMIP6 GCMs suggest. Internal variability, which can be estimated from a single-model initial condition large ensemble, adds uncertainty to the ice-free date (Jahn et al., 2016; Screen & Deser, 2019; Bonan et al., 2021) and implies an error range of approximately ± 8 years on these estimates. That is, under a high-emissions scenario, our constraint suggests that an ice-free September in the Arctic is 'likely' to occur between 2038–2053 and 'very likely' to occur between 2047–2063.

The same observational constraints can be applied under medium- and low-emissions scenarios. CMIP6 GCMs in conjunction with Eq. (1) suggest the 'likely' date of an ice-free Arctic in September occurs in 2064 and 2100 for medium- and low-emissions scenarios, respectively (Fig. 3b-c). Applying the same observational constraints on $\overline{A}_c$ and γ shifts this date to 2051 and 2091 for medium- and low-emissions scenarios, respectively. In both the medium- and low-emissions scenarios, correcting for mean-state biases pushes back the date of an ice-free Arctic. The observed local sea ice sensitivity moves forward the date of ice-free conditions for the medium-emissions scenario, but it does relatively little to the low-emission scenario. In both scenarios, the future evolution of the local sea ice sensitivity (diagnosed separately for each emissions scenario) moves forward the date of an ice-free

Arctic. When compared to the CMIP6 output, the constraints shift the 'as likely as not' (>33% probability) date for the medium-emissions scenario forward by approximately 7 years and the 'likely' date forward by approximately 15 years (Fig. 3b).

3.2 Late summer and early fall

Seasonality of an ice-free Arctic (Jahn, 2018; Niederdrenk & Notz, 2018; Årthun et al., 2021) is a feature of Arctic SIA projections that remains less quantified. Under a high emissions scenario, CMIP6 GCMs suggest that by 2081 the Arctic will 'likely' experience ice free conditions in July (Fig. 4a). Applying the same constraints on $\overline{A}_c$ and γ for July suggests the 'likely' date of an ice-free July is actually 2051, approximately 30 years sooner than GCMs suggest. This is related to the fact that GCMs have large biases in $\overline{A}_c$ and γ in July when compared to observations. Internal variability changes this estimate to between 2044 and 2058. For August, a similar picture emerges. CMIP6 GCMs suggest the Arctic will 'likely' experience ice free conditions in August by 2058, but the constrained estimate is 2048 with a range of 2043 and 2053 due to internal variability (Fig. 4b). The 'very likely' year is around 2056. All of these estimates are 10–30 years sooner than the GCMs suggest and the 'very likely' date moves forward by almost 50 years. October shows a similar picture to the other months. The 'likely' year of the Arctic experiencing ice-free conditions is 2070 (Fig. 4d). Observational constraints of $\overline{A}_c$ and γ moves forward this year to 2059, more than 10 years sooner than most GCMs suggest. The 'very likely' date is around 2071, which is approximately 30 years sooner than raw GCM projections.

Under SSP2-4.5 these constraints suggest the 'likely' date when the Arctic will experience an ice-free July occurs around 2058 (Fig. 4a). For SSP1-2.6, by the end of the 21st century it is 'as likely as not' that the Arctic will experience ice-free conditions in July. Furthermore, the probability of seeing ice-free conditions from July to October is greatly increased when compared to the raw output and will 'likely' occur around 2080 for a medium-emissions scenario. For a low-emissions scenario, at the end of the 21st century, the Arctic will 'likely' be ice free in September but not in other months. This suggests that the emissions scenario matters for the length of the ice-free season.

4 Discussion

While previous studies have also reduced the intermodel spread in Arctic SIA projections (Wang & Overland, 2009; Boé et al., 2009; Massonnet et al., 2012; Notz & SIMIP Community, 2020), most have done so by neglecting GCMs that poorly simulate present-day Arctic sea ice. The fact that GCMs can match observations for the wrong reasons (e.g., Rosenblum & Eisenman, 2017) suggests studies examining future projections should apply physically meaningful and robust constraints, rather than neglecting GCMs that do not meet certain observational criteria. This may explain why our results differ from the conclusions of Notz & SIMIP Community (2020), which find that after applying observational constraints even under a low-emissions scenario the majority of GCMs become ice-free by mid-century. Here, we find under a low-emissions scenario, the majority of GCMs instead become ice-free by 2082. These differences likely arise because we retain more intermodel differences in the simulated amount of Arctic warming.

This work, however, requires a few caveats. There are uncertainties associated with our observational estimates of Arctic warming and Arctic SIA that may change how well GCMs match observations, and change our observational estimates of γ, particularly at monthly timescales (Niederdrenk & Notz, 2018). We also did not explore the role of model inter-dependency (e.g., Sanderson et al., 2015; Knutti et al., 2017) on these conclusions. Investigation of how uncertainty in observations and model inter-dependency influence the results here should be the subject of future work.

5 Summary

This study introduces a simple framework to explain and constrain model projections of Arctic SIA over the 21st century. We find that a simple model (Eq. 1), which approximates future SIA based on present SIA and the sensitivity of SIA to Arctic temperatures, is able to emulate the evolution of Arctic SIA with remarkable skill. This model accounts for 70–95% of the intermodel variance in projections of Arctic SIA. Isolating the contributing factors shows that the majority of the model uncertainty in projections of Arctic SIA arises from biases in simulating present-day Arctic SIA. The remaining model uncertainty arises from differences in the simulated amount of Arctic warming, with some contribution from differences in the local sea ice sensitivity. While it is unclear whether Arctic temperatures are driving sea ice loss, or vice-versa, it does suggest that climate sensitivities (e.g., Meehl

et al., 2020) and representation of clouds in these GCMs (e.g., Zelinka et al., 2020) may be key to understanding the fate of Arctic sea ice.

Using observations to constrain the individual components of Eq. (1) moves forward the date of an ice free Arctic by 10–35 years. Under a high-emissions scenario, the probability of seeing ice-free conditions in the Arctic in September around 2035 is 'as likely as not', and the probability of seeing ice-free conditions in the Arctic in September around 2068 is 'virtually certain', which is much sooner than climate models suggest. The fate of Arctic sea ice throughout the summertime is similar. The probability of seeing ice-free conditions from July to October around 2059 is 'likely', and it is 'very likely' that the Arctic will experience ice-free conditions that persist from July to October around 2070 under a high-emissions scenario. Whereas previously it was widely believed that the Arctic will be ice free in September by mid-century under high emissions (Holland et al., 2006; Boé et al., 2009; Liu et al., 2013; Jahn, 2018; Niederdrenk & Notz, 2018; Sigmond et al., 2018; Notz & SIMIP Community, 2020), our work suggests that it is more likely that the Arctic will be ice free from July to October, not just in September. Importantly, by mid-century these dates shift under reduced emissions scenarios. Under a medium-emissions scenario, the Arctic will 'likely' only experience ice-free conditions from July to October after 2080. Under a low-emissions scenario, the Arctic will 'likely' only be ice free in September at the end of the 21st century. These results suggest the emissions scenario determines the length of the ice-free season. Overall, our results paint a dire picture of Arctic sea ice loss, implying ice-free summers in the Arctic are approaching faster than previously thought.

6 Methods

6.1 Observations

Monthly Arctic SIA from 1979 to 2020 was derived using observations of monthly sea ice concentration from the National Snow and Ice Data Center passive microwave retrievals bootstrap algorithm (Fetterer et al., 2016). For observation-based data of near-surface air temperature in the Arctic, we use the ERA5 global reanalysis (Hersbach et al., 2020). We use reanalysis data due to sparse data coverage of the Arctic toward the beginning of the satellite era. Monthly Arctic temperatures from 1979 to 2020 are obtained by calculating the average near-surface air temperature from 60°N to 90°N.

6.2 CMIP6 and large ensemble output

This analysis includes all CMIP6 GCMs (Eyring et al., 2016) that provide monthly output of sea ice concentration ('siconc') and near-surface air temperature ('tas') for Historical, SSP1-2.6, SSP2-4.5, and SSP5-8.5 simulations (29 different GCMs; see Supplementary Table 1). The Historical simulations (1850–2014) are merged with the SSP simulations (2015–2100). For each GCM, we use sea ice concentration to compute monthly Arctic SIA. Arctic temperatures are calculated as the average near-surface air temperature from 60°N to 90°N. We focus on single ensemble members from each GCM to mitigate over-weighting with respect to one GCM.

We also use the 40-member Community Earth System Model Large Ensemble (CESM1-LE) (Kay et al., 2015) to quantify how internal variability impacts estimates of when the Arctic first becomes seasonally ice free. The CESM1-LE uses RCP8.5 forcing, which differs slightly from the SSP5-8.5 forcing in the CMIP6 GCMs, but we expect the representation of internal variability under the RCP8.5 and SSP5-8.5 foricng to be similar. From each member we use sea ice concentration to compute monthly SIA and calculate Arctic-wide temperatures as the average near-surface air temperature from 60°N to 90°N.

6.3 Components of the simple model

Eq. (1) contains three components that are diagnosed from observations and the CMIP6 GCMs. The average Arctic SIA for a specific reference period $\overline{A}_c$ is calculated as the time-mean Arctic SIA from 1979–2020 for each month in all GCMs and in observations. The local sea ice sensitivity γ is defined as the change of SIA per degree of Arctic (60°N–90°N) warming. This formulation enables us to capture inter-annual variability of SIA related to Arctic temperature variability that is not captured when using the global-mean (Winton, 2011) or Northern Hemisphere mean (Armour et al., 2011). For each month, γ is computed using total least squares regression from 1979–2020 in observations and 1979-2100 in the CMIP6 GCMs for all values of SIA above 1 million km^2 following, Winton, (2011). For Figure 1, γ is calculated from 1979–2020 for each month using the observed Arctic SIA and Arctic temperatures obtained from ERA5. For Figure 2, γ is calculated from the GCMs over the Historical and SSP5-8.5 period from 1979–2100. For Figures 3–4, γ is calculated from 1979–2100 to produce the black line. Given that GCMs show more negative values of γ in the future, we further approximate γ from 1979 to a particular year until the end of the

21st century to obtain the future evolution of γ in GCMs. Figure S6 shows how the local sea ice sensitivity for each GCM evolves in time from 1979 up to the particular date for the months of July, August, September, and October. This is used to produce the red line in Figures 3 and 4 (which is further detailed below). $\overline{T}_c$ is the average Arctic temperature from 1979–2020 in each GCM and in observations, and $T(t)$ is the Arctic temperature for a given year and month.

6.4 Analysis of variance

The ability of Eq. (1) to explain the intermodel spread in CMIP6 Arctic SIA projections (Fig. 2a) is computed as the proportion of the variance (r^2, where r is the Pearson correlation coefficient) in monthly Arctic SIA from CMIP6 GCMs that is explained by Eq. (1) as a function of year and month. To examine the contribution of each term in Eq. (1) to the intermodel spread of Arctic SIA projections (Fig. 2b-d), we use the propagation of uncertainty to quantify the effect of uncertainty from each variable on the total uncertainty. Specifically, we apply the full intermodel spread of one term and hold the other two terms at their multi-model mean values yielding three sets of time series for $A(t)$, each containing 29 realizations, which are the result of the intermodel spread of each individual term. Assuming linearity, the total variance for a given month m and year y is:

$$T(m, y) = M(m, y) + S(m, y) + W(m, y) \tag{2}$$

where the fractional uncertainty from a given source is calculated as M/T, S/T, and W/T. M is calculated as the variance due to the intermodel spread in $\overline{A}_c$, S is calculated as the variance due to the intermodel spread in γ, and W is calculated as the variance due to the intermodel spread in $T(t) - \overline{T}_c$. The covariance terms are small and vary between 5–31%, which can be confirmed by calculating the residual between Fig. 2a and the variance explained by the sum of the three individual terms.

6.5 Probability density functions

The date of an ice-free Arctic is taken to be the first year when SIA falls below the 1 million km^2 threshold (Wang & Overland, 2009). This threshold, rather than zero, is commonly used since some sea ice may remain along the northern coasts of Greenland and Ellesmere Island after the bulk of the Arctic Ocean becomes open water. Assuming a

Gaussian distribution, the probability can be obtained as:

$$P\left(t_1 < t < t_2\right) = \int_{t_1}^{t_2} f(t)dt = \int_{t_1}^{t_2} \frac{1}{\sqrt{2\pi\sigma^2}} e^{\frac{-(t-\mu)^2}{2\sigma^2}} dt \tag{3}$$

where μ is the multi-model mean of the CMIP6 GCMs, σ is the standard deviation of all CMIP6 GCMs, and t is the ice-free date. Because some GCMs do not project ice-free conditions in the 21st century, each probability is normalized by the number of GCMs used relative to the total number of GCMs, which makes this analogous to the cumulative frequencies of GCMs being ice-free. In this paper, we adopt the IPCC likelihood scale where 'very unlikely' means 0–10%, 'unlikely' means 0–33%, 'as likely as not' means 33–66%, 'likely' means 66–100%, and 'very likely' means 90–100%. In Figures 3–4, the black line is the cumulative probability density function using Eq. (1) and the raw CMIP6 output. In Figure 3, the blue line is the cumulative density function after Eq. (1) is adjusted to have $\overline{A}_c$ be equal to the average September Arctic SIA from observations (1979–2020); the purple line is the same formulation as the blue line, but also with the observed γ for each month as estimated using the total least squares regression from observations (1979–2020); and the red line is the same as the blue and purple line, except that it contains guidance from the GCMs on how γ evolves in the future since for individual months it is not constant in time (see Fig. S6). Here γ is estimated from total least squares regression from 1979 to a particular date in each each month to obtain the future evolution of γ according to GCMs. Normalizing the multi-model mean of these timeseries with observations by dividing by the first value and multiplying by the observed value constrains the GCMs based on the observed sensitivity and guides the equation how γ evolves into the future. The red shading in Figure 3 indicates the estimate of internal variability from CESM1-LE, which is calculated as the two standard deviation of the CESM1-LE probability (see Fig. S5).

Acknowledgments

The authors thank Elizabeth Hunke, Caroline Holmes, and Francois Massonnet for helpful comments on an earlier draft of this work. The data that support the findings of this study are openly available at the following URL: https://esgf-node.llnl.gov/search/cmip6/. D.B.B. was supported by an American Meteorological Society (AMS) Graduate Fellowship and the National Science Foundation Graduate Research Fellowship Program (NSF Grant DGE-1745301). Part of this research was supported by Eric and Wendy Schmidt by recommendation of the Schmidt Futures program. I.E. acknowledges support from the National

Science Foundation (Grant OPP-1643445). R.C.J.W also acknowledges support from the National Science Foundation (Grant AGS-1929775).

References

Armour, K., Eisenman, I., Blanchard-Wrigglesworth, E., McCusker, K., & Bitz, C. (2011). The reversibility of sea ice loss in a state-of-the-art climate model. *Geophysical Research Letters*, *38*(16), L16705.

Årthun, M., Onarheim, I. H., Dörr, J., & Eldevik, T. (2021). The seasonal and regional transition to an ice-free Arctic. *Geophysical Research Letters*, *48*(1), e2020GL090825.

Boé, J., Hall, A., & Qu, X. (2009). September sea-ice cover in the Arctic Ocean projected to vanish by 2100. *Nature Geoscience*, *2*(5), 341–343.

Bonan, D. B., Lehner, F., & Holland, M. M. (2021). Partitioning uncertainty in projections of Arctic sea ice. *Environmental Research Letters*, *16*(4), 044002.

Davy, R., & Outten, S. (2020). The Arctic surface climate in CMIP6: status and developments since CMIP5. *Journal of Climate*, *33*(18), 8047–8068.

Diebold, F. X., & Rudebusch, G. D. (2021). Probability assessments of an ice-free Arctic: Comparing statistical and climate model projections. *Journal of Econometrics*.

Eyring, V., Bony, S., Meehl, G. A., Senior, C. A., Stevens, B., Stouffer, R. J., & Taylor, K. E. (2016). Overview of the Coupled Model Intercomparison Project Phase 6 (CMIP6) experimental design and organization. *Geoscientific Model Development*, *9*(5), 1937–1958.

Fetterer, F., Knowles, K., Meier, W., Savoie, M., & Windnagel, A. (2016). *Sea Ice Index, Version 3. Boulder, Colorado USA. NSIDC: National Snow and Ice Data Center.*

Ford, J. D., & Smit, B. (2004). A framework for assessing the vulnerability of communities in the Canadian Arctic to risks associated with climate change. *Arctic*, 389–400.

Gregory, J. M., Stott, P., Cresswell, D., Rayner, N., Gordon, C., & Sexton, D. (2002). Recent and future changes in Arctic sea ice simulated by the HadCM3 AOGCM. *Geophysical Research Letters*, *29*(24), 2175.

Hall, A., Cox, P., Huntingford, C., & Klein, S. (2019). Progressing emergent constraints on future climate change. *Nature Climate Change*, *9*(4), 269–278.

Hersbach, H., Bell, B., Berrisford, P., Hirahara, S., Horányi, A., Muñoz-Sabater, J., ... others (2020). The ERA5 global reanalysis. *Quarterly Journal of the Royal Meteorological Society*, *146*(730), 1999–2049.

Holland, M. M., Bitz, C. M., & Tremblay, B. (2006). Future abrupt reductions in the summer Arctic sea ice. *Geophysical Research Letters*, *33*(23), L23503.

Jahn, A. (2018). Reduced probability of ice-free summers for 1.5°C compared to 2°C warming. *Nature Climate Change*, *8*(5), 409–413.

Jahn, A., Kay, J. E., Holland, M. M., & Hall, D. M. (2016). How predictable is the timing of a summer ice-free Arctic? *Geophysical Research Letters*, *43*(17), 9113–9120.

Kay, J. E., Deser, C., Phillips, A., Mai, A., Hannay, C., Strand, G., ... others (2015). The Community Earth System Model (CESM) large ensemble project: A community resource for studying climate change in the presence of internal climate variability. *Bulletin of the American Meteorological Society*, *96*(8), 1333–1349.

Knutti, R., Sedláček, J., Sanderson, B. M., Lorenz, R., Fischer, E. M., & Eyring, V. (2017). A climate model projection weighting scheme accounting for performance and interdependence. *Geophysical Research Letters*, *44*(4), 1909–1918.

Laidre, K. L., Stirling, I., Lowry, L. F., Wiig, Ø., Heide-Jørgensen, M. P., & Ferguson, S. H. (2008). Quantifying the sensitivity of Arctic marine mammals to climate-induced habitat change. *Ecological Applications*, *18*(sp2), S97–S125.

Liu, J., Song, M., Horton, R. M., & Hu, Y. (2013). Reducing spread in climate model projections of a September ice-free Arctic. *Proceedings of the National Academy of Sciences*, *110*(31), 12571–12576.

Mahlstein, I., & Knutti, R. (2012). September Arctic sea ice predicted to disappear near 2°C global warming above present. *Journal of Geophysical Research: Atmospheres*, *117*(D6), D06104.

Massonnet, F., Fichefet, T., Goosse, H., Bitz, C. M., Philippon-Berthier, G., Holland, M. M., & Barriat, P.-Y. (2012). Constraining projections of summer Arctic sea ice. *The Cryosphere*, *6*(6), 1383–1394.

Meehl, G. A., Senior, C. A., Eyring, V., Flato, G., Lamarque, J.-F., Stouffer, R. J., ... Schlund, M. (2020). Context for interpreting equilibrium climate sensitivity and transient climate response from the CMIP6 Earth system models. *Science Advances*, *6*(26), eaba1981.

Melia, N., Haines, K., & Hawkins, E. (2016). Sea ice decline and 21st century trans-Arctic shipping routes. *Geophysical Research Letters*, *43*(18), 9720–9728.

Niederdrenk, A. L., & Notz, D. (2018). Arctic sea ice in a 1.5°C warmer world. *Geophysical Research Letters*, *45*(4), 1963–1971.

444 Notz, D. (2015). How well must climate models agree with observations? *Philosophical*
445 *Transactions of the Royal Society A: Mathematical, Physical and Engineering Sci-*
446 *ences*, *373*(2052), 20140164.

447 Notz, D., & Marotzke, J. (2012). Observations reveal external driver for Arctic sea-ice
448 retreat. *Geophysical Research Letters*, *39*(8).

449 Notz, D., & Stroeve, J. (2016). Observed Arctic sea-ice loss directly follows anthropogenic
450 CO2 emission. *Science*, *354*(6313), 747–750.

451 Notz & SIMIP Community. (2020). Arctic Sea Ice in CMIP6. *Geophysical Research Letters*,
452 *47*(10), e2019GL086749.

453 Olonscheck, D., Mauritsen, T., & Notz, D. (2019). Arctic sea-ice variability is primarily
454 driven by atmospheric temperature fluctuations. *Nature Geoscience*, *12*(6), 430–434.

455 Overland, J. E., & Wang, M. (2013). When will the summer Arctic be nearly sea ice free?
456 *Geophysical Research Letters*, *40*(10), 2097–2101.

457 Rosenblum, E., & Eisenman, I. (2016). Faster Arctic sea ice retreat in CMIP5 than in
458 CMIP3 due to volcanoes. *Journal of Climate*, *29*(24), 9179–9188.

459 Rosenblum, E., & Eisenman, I. (2017). Sea ice trends in climate models only accurate in
460 runs with biased global warming. *Journal of Climate*, *30*(16), 6265–6278.

461 Sanderson, B. M., Knutti, R., & Caldwell, P. (2015). Addressing interdependency in a
462 multimodel ensemble by interpolation of model properties. *Journal of Climate*, *28*(13),
463 5150–5170.

464 Screen, J., & Deser, C. (2019). Pacific Ocean variability influences the time of emergence of
465 a seasonally ice-free Arctic Ocean. *Geophysical Research Letters*, *46*(4), 2222–2231.

466 Senftleben, D., Lauer, A., & Karpechko, A. (2020). Constraining uncertainties in CMIP5
467 projections of September Arctic sea ice extent with observations. *Journal of Climate*,
468 *33*(4), 1487–1503.

469 Shu, Q., Wang, Q., Song, Z., Qiao, F., Zhao, J., Chu, M., & Li, X. (2020). Assessment of
470 sea ice extent in CMIP6 with comparison to observations and CMIP5. *Geophysical*
471 *Research Letters*, *47*(9), e2020GL087965.

472 Sigmond, M., Fyfe, J. C., & Swart, N. C. (2018). Ice-free Arctic projections under the Paris
473 Agreement. *Nature Climate Change*, *8*(5), 404–408.

474 Snape, T. J., & Forster, P. M. (2014). Decline of Arctic sea ice: Evaluation and weighting of
475 CMIP5 projections. *Journal of Geophysical Research: Atmospheres*, *119*(2), 546–554.

476 Stroeve, J., Kattsov, V., Barrett, A., Serreze, M., Pavlova, T., Holland, M., & Meier,

W. N. (2012). Trends in Arctic sea ice extent from CMIP5, CMIP3 and observations. *Geophysical Research Letters*, *39*(16), L16502.

Stroeve, J., & Notz, D. (2018). Changing state of Arctic sea ice across all seasons. *Environmental Research Letters*, *13*(10), 103001.

Wang, M., & Overland, J. E. (2009). A sea ice free summer Arctic within 30 years? *Geophysical research letters*, *36*(7), L07502.

Winton, M. (2011). Do climate models underestimate the sensitivity of Northern Hemisphere sea ice cover? *Journal of Climate*, *24*(15), 3924–3934.

Wyllie-Echeverria, T., & Wooster, W. S. (1998). Year-to-year variations in Bering Sea ice cover and some consequences for fish distributions. *Fisheries Oceanography*, *7*(2), 159–170.

Zelinka, M. D., Myers, T. A., McCoy, D. T., Po-Chedley, S., Caldwell, P. M., Ceppi, P., ... Taylor, K. E. (2020). Causes of higher climate sensitivity in CMIP6 models. *Geophysical Research Letters*, *47*(1), e2019GL085782.

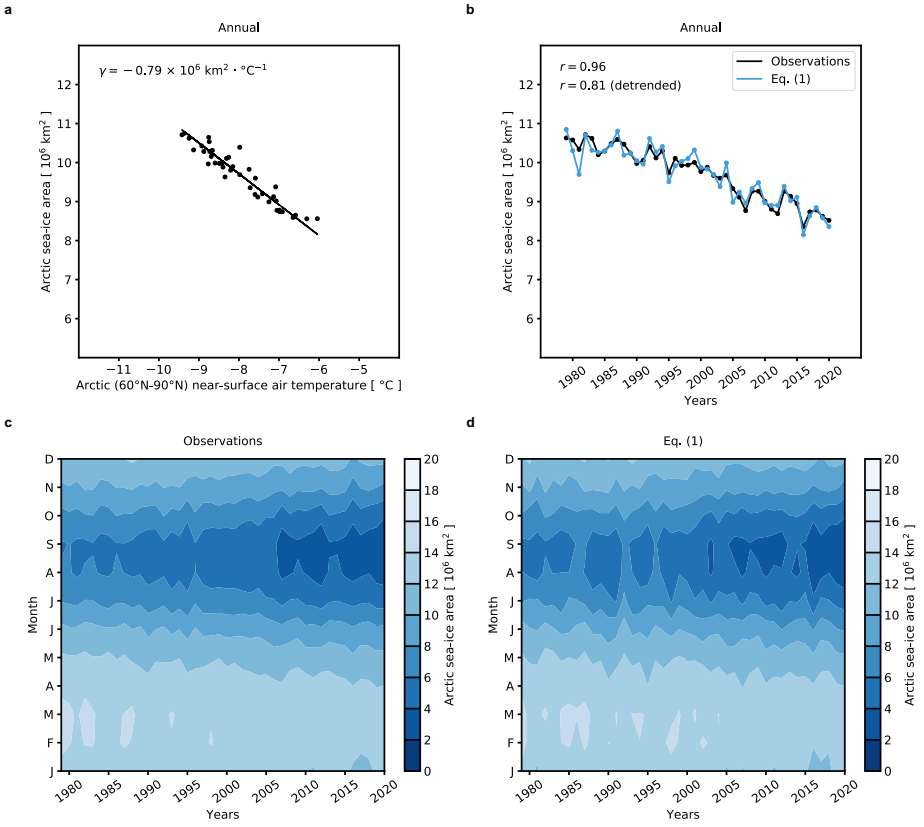

Figure 1. Applying the simple model (Eq. 1) to observations. (a) Scatter plot showing the relationship between observed annual Arctic (60°–90°N) near-surface air temperature and annual Arctic sea-ice area from 1979–2020, implying a local sea ice sensitivity of $\gamma = -0.79 \times 10^6$ km^2 °C^{-1}. (b) Annual Arctic sea-ice area from 1979–2020 in observations (black) and using Eq. (1) with observed temperature variations (blue). The correlation between the two time series is shown in the upper left with and without the linear trend. Monthly Arctic sea-ice area from 1979–2020 in (c) observations and (d) using Eq. (1) with γ estimated for each month.

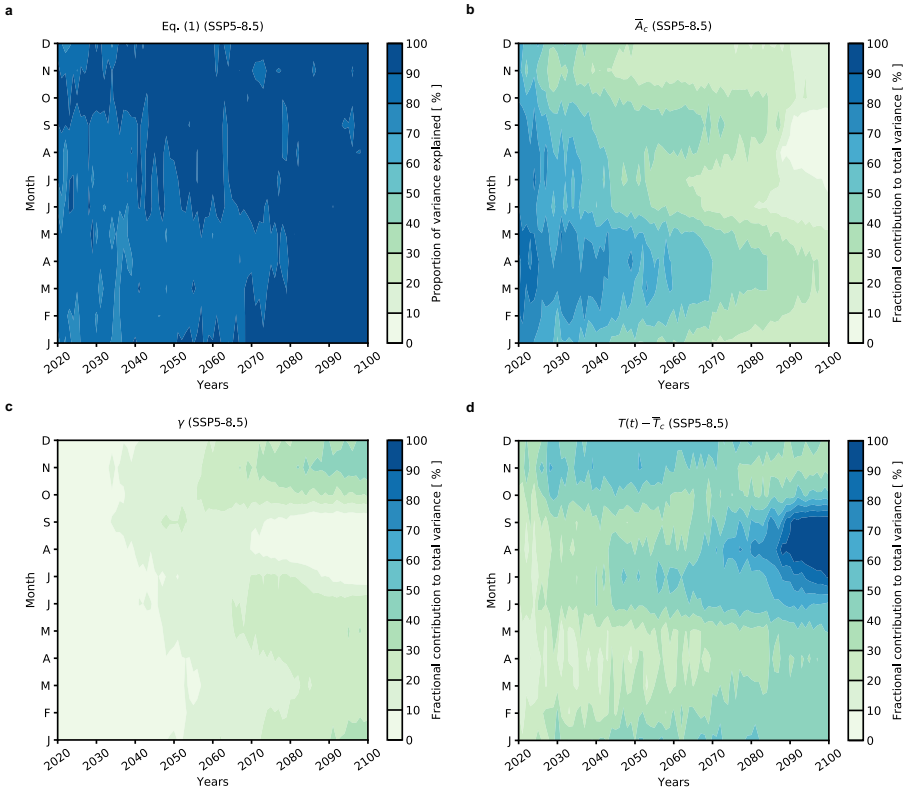

Figure 2. Partitioning intermodel variance in projections of Arctic sea-ice area. (a) The proportion of the intermodel variance (r^2, where r is the Pearson correlation coefficient) in monthly Arctic sea-ice area from CMIP6 SSP5-8.5 simulations that is accounted for by Eq. (1) as a function of month and year. Fractional contribution of (b) $\overline{A}_c$, (c) γ, and (d) $T(t) - \overline{T}_c$ to the total variance for SSP5-8.5 as a function of month and year.

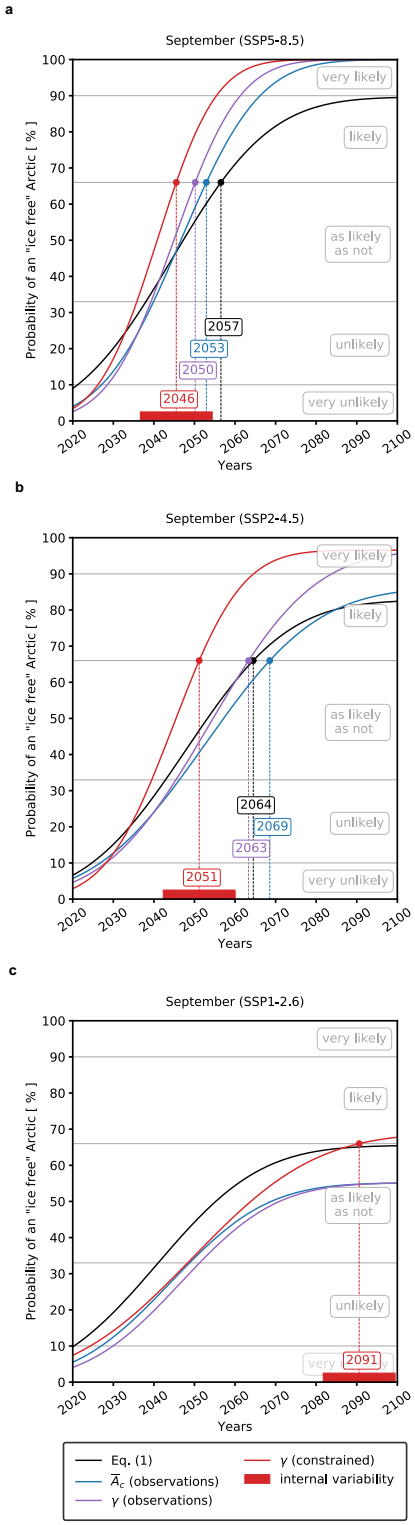

Figure 3. Probability of an ice-free Arctic in September. Cumulative probability density function for the year when the Arctic will experience ice free conditions in September for (a) SSP5-8.5, (b) SSP2-4.5, (c) SSP1-2.6. The black line is the unconstrained Eq. (1) using CMIP6. The blue line is constrained by the mean September Arctic sea-ice area from 1979–2020 in observations. The purple line is constrained by both the mean September Arctic sea-ice area and local sea ice sensitivity from 1979–2020 observations. The red line is the same as the purple line, but with guidance from the GCMs on how the local sea ice sensitivity evolves in the future. The red shading denotes the range due to internal variability estimated from the CESM1-LE.

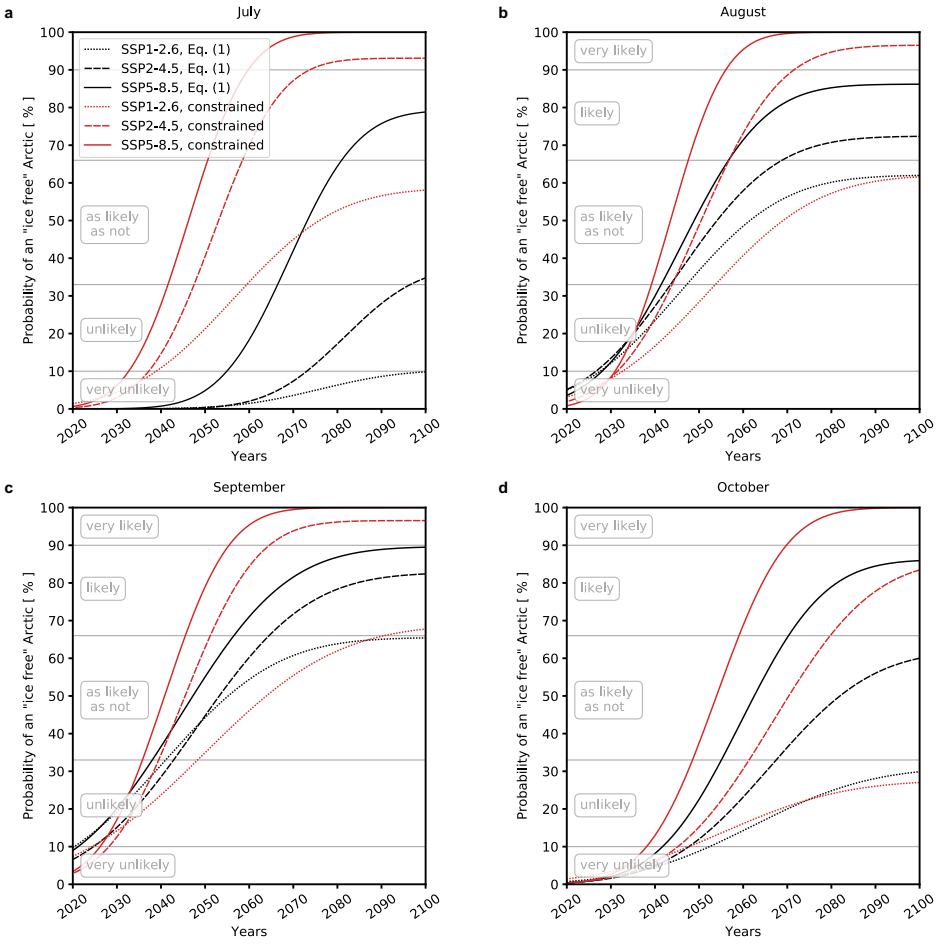

Figure 4. Probability of an ice-free Arctic from July to October. Cumulative probability density function for the year when the Arctic will experience ice free conditions in (a) July, (b) August, (c) September, and (d) October. The black line is the unconstrained Eq. (1) using CMIP6. The red line is the constrained output with the observed $\overline{A}_c$ and γ, and with guidance on how the local sea ice sensitivity evolves in the future (as in Figure 3). The solid lines, dashed lines, and dotted lines denote SSP5-8.5, SSP2-4.5, and SSP1-2.6, respectively.